


**Multidirectional switching behavior by transversely stretching a composite cholesteric elastomer**Guillermo Reyes \* and Juan Adrián Reyes*Física Química, Instituto de Física, Universidad Nacional Autónoma de México, México D.F. 04510, México*

(Received 3 December 2019; revised 27 August 2020; accepted 1 September 2020; published 23 September 2020)

We have analyzed the propagation of electromagnetic waves impinging obliquely in a hybrid material, made by a cholesteric elastomer slab with spherical metallic inclusions randomly located in the host material. We have carried out an analytical and numerical model which permits us to obtain the reflection and transmission spectra when the system is submitted to a mechanical stress applied transversely to the cholesteric axis. We have demonstrated that for a large interval of angles of incidence, it can be observed a switching behavior from a discriminatory circular filter to a polarization independent device. The sample also exhibits regions of transformation from right to left circularly polarized waves in the reflection spectra, which are intercalated with zones of similar transmission of both circularly polarized waves.

DOI: [10.1103/PhysRevE.102.032702](https://doi.org/10.1103/PhysRevE.102.032702)**I. INTRODUCTION**

Cholesteric liquid crystalline elastomers (CLCEs) are soft solids made of mesogenic molecules embodied into a polymer backbone with helical arrangement resembling low-molecular-weight chiral nematic liquid crystals [1]. The interaction between the polymer chains and mesogens relates orientational order of the mesogens to mechanical strain applied to the polymer chains. Such an interrelationship induces a range of electro-mechanical and opto-mechanical phenomena, with a great range of possible applications [2]. Tunable lasing from a single CLCE film was observed for the first time and reported in 2001 [3]. It was found that by extensively stretching the elastomer film, the cholesteric pitch is reduced, causing a noticeable redshift of the reflection band and, in turn, of the wavelength of laser emission. Additionally the pitch of the CLCE was switched by applying a biaxial strain normal to the helical axis. This deformation diminishes the helical pitch, keeping the 1D structure completely invariant, but giving rise to a nonvanishing distortion with supplementary shear near the sample borders. As a consequence, the helical pitch varies across the cholesteric elastomer film, and its meticulous ascertainment is difficult.

Liquid crystals behave as photonic crystals, so they show an optical band gap in their reflectance and transmittance spectra. Given that an LCE combines the optical properties of the liquid crystals and the mechanical properties of elastomers, the band gap can be modified selectively if the LCE gets deformed. Whether the magnitude of the stress applied is sufficiently large, the LCE will show a bandwidth in a different wavelength range; moreover the form of the optical band gap observed will be different. These results have been reported in various experiments, for instance, in cholesteric liquid crystalline polymer films, where selective transmission and reflection under biaxial stress have been detected; the

same behavior also has been observed in stretchable liquid-crystal blue-phase gels [4,5]. Furthermore, other authors have found solutions to boundary value problems corresponding to electromagnetic waves impinging normally with respect to transverse section of a cholesteric elastomer using numerical methods [6].

The method of mechanical tuning of the lasing wavelength for single, or layered, CLCEs consists in setting a uniaxial extension on the cholesteric elastomer film that is applied in the orthogonal direction with respect to the helical axis. The uniaxial elongation, perpendicular with respect to the helical axis of cholesteric elastomer, induces an extension parallel to the strain, and a contraction that follows a power law along the remaining perpendicular directions. This phenomenon has been widely analyzed theoretically [7,8], and measured experimentally [9]. The cholesteric director is gradually aligned with the applied strain, and it produces a remarkable deformation of the cholesteric helix, that is to say, the molecules of liquid crystal linked with polymers will change their orientations.

Furthermore, the presence of metallic inclusions produces a remarkable modification in the transmittance and reflectance spectra of the sample because of the occurrence of the plasmon resonance phenomenon. This has been reported for a nanocomposite consisting of metallic nanospheres randomly dispersed in a transparent matrix, whereas the optical properties of host materials lack resonant properties [10]. In addition, many periodic chiral dielectric and metallic structures have been studied for some years because of its ability to provide giant circular dichroism [11–13] or giant optical activity even for the optical regime. Nowadays, with energy losses, chiral dielectric structures overcome the expectations of chiral metallic structures by a large margin. Moreover, various works have demonstrated that the photonic band gap can be dramatically deformed by including metallic dispersive inclusions [14–16]. For instance, a graphene photonic band structure can be tailored by inserting metallic sheets [17]. Also, a system possessing a nonchiral band gap for which gold helices have been inserted can act as a circular polarizer

\*reyesvalgui@gmail.com

of the same handedness of the helices [18]. Also, the optical properties of a cholesteric liquid crystal (CLC), doped with a dye, have been studied recently [19], and it was shown that the presence of dye molecules splits the photonic band gap of the CLC, into two, three, or even more band gaps under certain conditions. Also, the Bragg frequencies and the widths of forbidden bands can be varied by changing the parameters of dye molecules.

Different studies have been carried out about the spectral properties of a CLC with a combined defect, which consists of a layer made of metallic nanospheres, which are dispersed in a transparent matrix layer and a twist jump [20–22]. It was found that the band-gap width and the position of defect modes can be controlled by external fields applied to the cholesteric liquid crystal. A recent study of sculptured thin films doped with metallic spheres has shown that if the position of the resonance frequency of the dopant is located inside the pure helical band gap, the bands split and new sub-band gaps are created [23].

Other studies of the optical spectra of CLCEs have been performed for elastomers under the action of an axial strain [24]. Subsequently, a generalization for calculating the optical spectra for oblique incidence was developed, where an omnidirectional reflection band appears induced by the metallic resonance [25]. An elastomer transversely stretched also doped with metallic inclusions was analyzed previously [26]. It is worth mention that when a cholesteric elastomer is transversely stretched, the system is deformed in such a way that the discriminatory circular features of the material are gradually lost after a critical strain. Therefore, intervals of conversion from right to left circularly polarized waves can be observed in the reflection spectra. These intervals are alternated with regions resembling the transmission spectra for both circularly polarized waves, whereas the zones near the metallic resonance are damped.

In this paper, we carry out theoretical and numerical research to study the behavior of electromagnetic waves impinging in any direction with respect to the boundary of a cholesteric elastomer sample in order to discern which of the features mentioned above are present for other angles of wave propagation. The sample is doped with silver nanospheres uniformly and randomly distributed in the structure. As a consequence of the presence of metallic spheres, the optical response is modified. Moreover, the slab is transversely stretched by the action of mechanical forces.

## II. ELASTIC MODEL

Let us assume an elastomer submitted to an external stretch imposed transversely to the pitch axis; the system is elongated

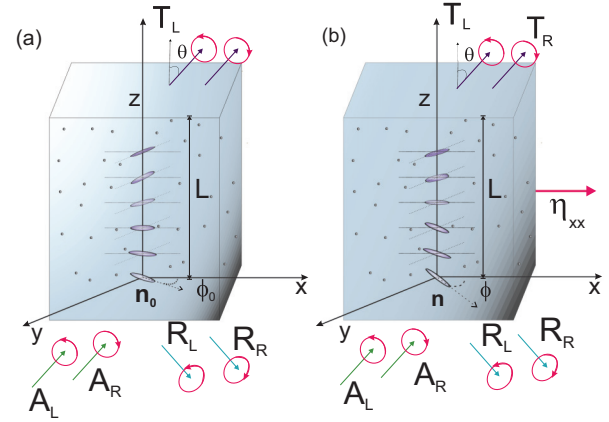


FIG. 1. Schematic of the system. An electromagnetic field is shown as it impinges on an elastomer cholesteric slab of finite thickness: panel (a) corresponds to an undistorted elastomer, and panel (b) to an elastomer under action of a force.

uniformly in the direction  $x$ , and this strain is denoted by  $\eta_{xx} = \eta$ . It is reasonable to expect that the rotations of the director vector have to be confined to the plane  $x$ - $y$ . However, the strains  $\eta_{xy}$  and  $\eta_{yx}$ , which give rise to soft elasticity, are suppressed. The strains  $\eta_{xz}$ , and  $\eta_{yz}$  are not involved because of symmetry reasons, even though they are not subjected to compatibility requirements. Before the deformation, the corresponding director can be written as

$$\hat{\mathbf{n}}_0 = (\cos \phi_0, \sin \phi_0, 0), \quad (1)$$

where  $\phi_0 = q_0 z$ ,  $q_0$  represents the chiral wave number, with  $q_0 = \frac{2\pi}{p}$ , and  $p$  is the spatial period of the structure, which is a function of different physical variables as temperature and material composition, and  $z$  denotes the position along the elastomer. Since the deformation occurs in a direction transverse to the cholesteric axis, the director rotates after the deformation, but stays in  $x$ - $y$  plane, to yield

$$\hat{\mathbf{n}} = (\cos \phi, \sin \phi, 0), \quad (2)$$

where  $\phi = \tilde{q}z$  and  $\tilde{q} = \frac{q_0}{\eta_{zz}}$ ,  $\eta_{zz}$  represents a strain due to contraction in the  $z$  direction because of the stretch  $\eta_{xx} = \eta$ . A system scheme is shown in Fig. 1. In Fig. 1(a) we can observe an undistorted LCE slab of length  $L$ , and in Fig. 1(b) it is shown an LCE under the action of a strain in the  $x$  direction. In both cases, electromagnetic waves are impinging obliquely in the slab, forming a  $\theta$  angle with respect to the cholesteric axis.

The spatial orientation of the mesogenic molecules after a deformation is obtained by minimizing the free energy density for an elastomer, which for a contraction orthogonal to the helix axis is given by

$$F_{\perp} = \frac{1}{2}C \left\{ \eta^2 + \eta_{yy}^2 + \eta_{zz}^2 + \frac{g-1}{4g} [(g-1)(\eta^2 + \eta_{yy}^2)(1 - \cos 2\phi \cos 2\phi_0) + (g+1)(\eta^2 - \eta_{yy}^2)(\cos 2\phi - \cos 2\phi_0) - 2(g-1)\eta\eta_y \sin 2\phi \sin 2\phi_0] \right\}. \quad (3)$$

Here  $C = 10^6$  Pa is the shear modulus of the elastomer and  $g = l_{\parallel}/l_{\perp}$  is the anisotropy ratio of the elastomer, which is a characteristic value of the polymer backbone. Indeed,  $g$  measures the shape anisotropy of the backbone, which, although coupled to the mesogens, might not have an identical degree of alignment. Thus, in liquid crystal polymers it is necessary to distinguish between the anisotropy of the polymer backbone and the orientational mesogenic order. To ensure the equilibrium of the system, we require the Helmholtz free energy density to be a minimum. Because of our last assumption, the free energy of this expression has to be minimized with respect to the director angle  $\phi$  at a given extension. Hence the director after the deformation depends on the initial director and is given by the

expression [26]

$$\tan 2\phi = \frac{2\eta\eta_{yy}(g-1)\sin 2\phi_0}{(g-1)(\eta^2 + \eta_{yy}^2)\cos 2\phi_0 + (g+1)(\eta^2 - \eta_{yy}^2)}. \quad (4)$$

The Frank energy is being neglected, hence the free energy is optimized at each point of  $z$ . The optimal strain perpendicular to the pitch  $\eta_{yy}$  minimizes the total free energy of half a helix repeat, given by the expression  $\langle F_{\perp} \rangle = \int_0^{\pi/2} d\phi_0 F_{\perp}$ . Taking  $\partial\langle F_{\perp} \rangle/\partial\eta_{yy}^2 = 0$  gives rise to the condition for  $\eta_{yy}$ , and by setting the preserved volume condition, we can obtain that  $\eta_{zz} = 1/\eta\eta_{yy}$ , and, finally, the condition for  $\eta_{yy}$  is given by [7,8]

$$\frac{\pi}{4} \frac{(g+1)^2}{g} - \frac{\pi}{\eta_{yy}^4 \eta^2} = \frac{g-1}{2g} \int_0^{\pi/2} d\phi_0 \frac{a_1[(g+1) - (g-1)\cos 2\phi_0]\cos 2\phi - 4g\eta^2}{\sqrt{a_1^2 - 4g\eta^2\eta_{yy}^2}}, \quad (5)$$

where we have straightforwardly integrated the terms not involving  $\cos 2\phi$  and  $\sin 2\phi$  and

$$a_1 = \frac{1}{2}[(g+1)(\eta^2 + \eta_{yy}^2) + (g-1)(\eta^2 - \eta_{yy}^2)\cos 2\phi_0]. \quad (6)$$

Equation (5) can be solved numerically. Alternatively, one can expand it for small strains,  $\eta - 1 \ll 1$ . It is then simple to show analytically that the strain in the  $y$  direction goes as  $\eta_{yy} \simeq \eta^{-5/7}$  and  $\eta_{zz} \simeq \eta^{-2/7}$ . This analytical approach to the transverse contraction provides a response, which is a compromise between classically hard ( $\eta_{yy} = \eta_{zz} \sim 1/\sqrt{\eta}$ ) and semisoft behavior ( $\eta_{yy} \sim 1/\eta$ ), meaning that at some points along the helix, the director rotates towards the stretching direction  $\hat{x}$  to reduce the cost in elastic energy, and at others it cannot, so it responds as if as hard as those points which already are along  $\hat{x}$ . The contraction transports the helix with it, so the pitch contracts by a factor  $\eta^{-2/7}$  and the wave number is  $q = \eta^{2/7}q_0$ .

The fact that the strains  $\eta_{xx} = \eta$  and  $\eta_{yy}$  are different makes the director of the liquid crystal rotate. Actually, these strains do not depend on  $z$ , so they have the same magnitude for every value of  $z$ . This is a consequence of the fact that the three nonvanishing elements of the strain tensor  $\eta_{xx}$ ,  $\eta_{yy}$ , and  $\eta_{zz}$ , were expressed in terms of the externally imposed strain  $\eta_{xx} = \eta$ . This in turn was established after minimizing  $\langle F_{\perp} \rangle$  with respect to the remaining free variable  $\eta_{yy}$ , as can be seen in the procedure developed above, provided the preserved volume condition is fulfilled. Thus, by assuming a uniform imposed element  $\eta$  we get a  $z$ -independent strain; nevertheless the cholesteric configuration, that is to say the orientation of the director, would not rotate by the same value for all  $z$  [see Eq. (4)]. Moreover, after a given threshold strain  $\eta_c$  (defined below) it will almost untwist.

Equation (4) also defines a characteristic value called  $\eta_c$ , which can be estimated examining Eq. (4) for  $\phi_0 = (\frac{\pi}{2})^{\pm}$ , where this expression denotes angles in a neighborhood of ( $\phi_0 = \frac{\pi}{2}$ ); hence a twist wall is defined, that is to say, a value that separates two possible states of rotation of the director:

rotation towards  $\phi = 0$  for the interval  $0 < \phi_0 < \frac{\pi}{2}$  and rotation towards  $\phi = \pi$  for the interval  $\frac{\pi}{2} < \phi_0 < \pi$ ; for  $\eta > \eta_c$  the twist wall disappears, and only exist one state for the rotation. The value  $\eta_c$  has the analytical form  $\eta_c \sim g^{7/24}$ , for  $\eta \sim 1$ . In this work we take  $g = 1.16$ , hence  $\eta_c = 1.04424$ , therefore we will study an elastomer submitted to different strains: in its undistorted state ( $\eta = 1$ ),  $\eta = 1.03$ , which is found in the range  $\eta < \eta_c$ , and finally  $\eta = 1.07$ , which is in the interval  $\eta > \eta_c$ ; the behavior of  $\phi$  versus  $z$ , for different values of  $\eta$ , can be found in Ref. [26].

Before ending this section, we shall compare our system with a piezo-electric-controlled polymeric sculptured thin film (STF) [27]. The optical response of an STF is governed by its permittivity matrix, which should be determined after being compressed by a piezo-electric slab. The compression modifies not only the value of STF pitch  $q$  but also the elements of the permittivity tensor, giving rise to a blueshift for the central wavelength of about 10 nm. Even though an LCE has a polymeric backbone, the mesogens attached to the polymer skeleton offer a significant contribution in the optical properties of the LCE. Hence, by stretching an LCE within the soft elasticity interval [7], the orientation of the mesogens is changed without changing its optical indexes. This implies that the permittivity tensor of an LCE depends on the resulting strains by means of the director  $\hat{n}$ . This peculiar behavior, so-called soft elasticity, is a consequence of the mechanical coupling between the low-density cross-linked polymer and the mesogenic molecules, which mathematically is manifested as a golden mode in the neoclassical free energy  $F$  to describe an LCE. This causes in turn that the energy required to stretch a LCE during the mesogenic reorientation is theoretically null but practically negligible.

### III. OPTICAL SPECTRA

An LCE can be treated as a uniaxial medium, and therefore the orientation angle of the mesogenic molecules determines the dielectric response; however, the presence of metallic inclusions makes necessary a theory of an effective medium

to find the effective permittivity of the hybrid medium. The effective response of a dielectric composite sample, produced by inserting a very small amount of an isotropic dopant randomly dispersed in an also isotropic homogeneous medium can be approximated by using a generalization the Maxwell Garnett formula for a locally uniaxial medium [28,29], which has been deduced by assuming the long-wavelength approximation. None of the physical parameters of the components of the hybrid medium change with the amplitude of the external field; moreover, neither of the physical quantities of the mixed medium is a function of time as a result of external forces. The characteristic scale of the dopant is shorter than the wavelength of light propagating in the composite medium. The guest medium is randomly dispersed, and the filling factor should be smaller than the percolation threshold, which means that there is no long-range connectivity among the parts of the particulated material.

The dielectric tensor for the effective uniaxial medium is given by the expression [30]

$$\tilde{\epsilon}^{\text{eff}} = \epsilon_{\perp}^e(\omega)\tilde{I} + [\epsilon_{\parallel}^e(\omega) - \epsilon_{\perp}^e(\omega)]\hat{\mathbf{n}}\hat{\mathbf{n}}, \quad (7)$$

where  $\epsilon_{\perp}$ , and  $\epsilon_{\parallel}$ , are the dielectric responses in the perpendicular and parallel directions with respect to the director vector.

The Maxwell Garnett approach has been generalized to study the dielectric response of locally uniaxial materials [31]. Expressions of general validity for getting the effective relative permittivity and permeability tensors have been calculated for the case when both the guest and host media are uniaxial. Both dielectric and magnetic tensors must be calculated simultaneously for the general case; nevertheless, the effective dielectric tensor can be considerably diminished when the dielectric anisotropy given by the ratio  $\frac{\epsilon_{\parallel}^h}{\epsilon_{\perp}^h}$  (where  $\epsilon_{\perp,\parallel}^h$  are the dielectric responses in the perpendicular and parallel directions with respect to the director vector for the host material) is approximately 1, which means that the terms of order up to  $O[(\epsilon_3 - \epsilon_1)/(\epsilon_3 + \epsilon_1)]^3$  can be ignored. For this case, the local effective permittivities are [32]

$$\epsilon_{\perp,\parallel}^e(\omega) = \epsilon_{\perp,\parallel}^h \left[ 1 + \frac{f}{\epsilon_{\perp,\parallel}^h / (\epsilon_m(\omega) - \epsilon_{\perp,\parallel}^h) + (1-f)/3} \right], \quad (8)$$

where  $\epsilon_m(\omega)$ , is the relative permittivity of the metallic inclusions. We are taking into account the Drude model for the metal nanospheres. This is stated by the expression

$$\epsilon_m(\omega) = \epsilon_0 - \frac{\omega_p^2}{\omega(\omega + i\gamma)}, \quad (9)$$

where  $\epsilon_0$  is the background dielectric constant taking into account contributions from interband transitions,  $\omega_p$  the plasma frequency,  $\gamma$  the plasma relaxation rate, and, as we mentioned above,  $\omega$  is the frequency of the propagating wave. Before proceeding with our discussion of the optical properties of this hybrid system, it is worth mention that the radius and shape of the metallic nanospheres remain practically unaffected after stretching the elastomer because the shear modulus  $C = 10^6$  Pa of the LCE is much smaller than the shear modulus of silver, the dopant material. One should bear in mind that the elastomer is submitted only to shear deformations, so neither the metal nor the elastomer changes their volumes.

In order to find the transmittance and reflectance spectra, we state the Maxwell equations in different regions: for  $z < 0$  we have both incident and reflected electromagnetic waves circularly polarized, and for  $z > L$  we have only circularly polarized transmitted waves.

For the region outside the LCE we have to solve the source-free Maxwell equations in the vacuum. For the region inside the LCE corresponding to  $0 < z < L$ , we also have to solve the source-free Maxwell equations; however, we will consider the constitutive relation for the displacement to be  $\mathbf{D}(\mathbf{r}) = \tilde{\epsilon}^{\text{eff}} \cdot \mathbf{E}(\mathbf{r})$ . Therefore, we state below the optical response in the three corresponding regions by means of the Maxwell equations.

#### A. Maxwell equations in the region outside the LCE

As has been stated in the last section, we will consider a circularly polarized electromagnetic wave which impinges a LCE slab of thickness  $L$  located at  $0 < z < L$ , whose helical axis is aligned parallel to the normal of the plane boundaries of the slab, which is surrounded by two semispaces of vacuum. In the first region, corresponding to vacuum for  $z < 0$ , the solution of the Maxwell equations can be expressed in terms of simple plane waves which we choose to be a linear combination of right and left circularly polarized waves. This expression is given by

$$\mathbf{E}(\mathbf{r}) = (A_R \mathbf{n}_{-1} + A_L \mathbf{n}_{+1}) \exp(i\mathbf{k}_1 \cdot \mathbf{r}) + (R_R \mathbf{n}_{-2} + R_L \mathbf{n}_{+2}) \exp(i\mathbf{k}_2 \cdot \mathbf{r}), \quad (10)$$

$$\mathbf{H}(\mathbf{r}) = \frac{1}{\mu_0 \omega} [\mathbf{k}_1 \times (A_R \mathbf{n}_{-1} + A_L \mathbf{n}_{+1}) \exp(i\mathbf{k}_1 \cdot \mathbf{r}) + \mathbf{k}_2 \times (R_R \mathbf{n}_{-2} + R_L \mathbf{n}_{+2}) \exp(i\mathbf{k}_2 \cdot \mathbf{r})], \quad (11)$$

where  $\omega$  indicates the wave frequency,  $\mathbf{k}_j = k_x \hat{\mathbf{x}} + k_y \hat{\mathbf{y}} - (-1)^j k_z \hat{\mathbf{z}}$ , ( $j = 1, 2$ ) are the forward and backwards wave vectors,  $\mu_0$  is the permeability of the vacuum,  $A_{L,R}$  are the amplitudes of the incident waves with right and left circularly polarizations, and  $R_{L,R}$  are the amplitudes of the reflected waves.

Here the unit vectors of the circularly polarized waves can be expressed as

$$\mathbf{n}_{\pm j} = \frac{(-1)^{j+1}}{\sqrt{2}} \left( \frac{[\hat{\mathbf{z}} \times \mathbf{k}_j] \times \mathbf{k}_j}{|\hat{\mathbf{z}} \times \mathbf{k}_j| k_j} \pm i \frac{\hat{\mathbf{z}} \times \mathbf{k}_j}{|\hat{\mathbf{z}} \times \mathbf{k}_j|} \right), \quad (12)$$

where the vectors  $\hat{\mathbf{z}} \times \mathbf{k}_j$  and  $[\hat{\mathbf{z}} \times \mathbf{k}_j] \times \mathbf{k}_j$  form a base for an incident  $\mathbf{E}(\mathbf{r})$  with linear polarization, and the vectors  $\mathbf{n}_{+1}$  and  $\mathbf{n}_{-1}$  play the same role for an incident wave whose polarization is circular. Analogously the vectors  $\mathbf{n}_{+2}$  and  $\mathbf{n}_{-2}$  form a base for the states of polarization of the reflected wave for  $z > L$ . Hence, the transmitted wave can be expressed as

$$\mathbf{E}(\mathbf{r}) = (T_R \mathbf{n}_{-1} + T_L \mathbf{n}_{+1}) \exp(i\mathbf{k}_1 \cdot \mathbf{r}) + (B_R \mathbf{n}_{-2} + B_L \mathbf{n}_{+2}) \exp(i\mathbf{k}_2 \cdot \mathbf{r}), \quad (13)$$

$$\mathbf{H}(\mathbf{r}) = \frac{1}{\mu_0 \omega} [\mathbf{k}_1 \times (T_R \mathbf{n}_{-1} + T_L \mathbf{n}_{+1}) \exp(i\mathbf{k}_1 \cdot \mathbf{r}) + \mathbf{k}_2 \times (B_R \mathbf{n}_{-2} + B_L \mathbf{n}_{+2}) \exp(i\mathbf{k}_2 \cdot \mathbf{r})], \quad (14)$$

where  $T_{R,L}$  are the transmission amplitudes and  $B_{R,L}$  can be understood as incident amplitudes coming from the right side,

in the region  $z > L$ . In our case we set  $B_R = B_L = 0$ . Additionally, we will construct the four-dimension vector  $\boldsymbol{\psi}(z)$ , whose components are those of the transverse electric and magnetic fields

$$\boldsymbol{\psi}(z) = \begin{pmatrix} E_x(z) \\ E_y(z) \\ B_x(z) \\ B_y(z) \end{pmatrix}. \quad (15)$$

We write Maxwell equations in the absence of sources in SI units

$$\nabla \cdot \mathbf{D}(\mathbf{r}) = 0, \quad (16)$$

$$\nabla \times \mathbf{E}(\mathbf{r}) = \iota\omega\mathbf{B}(\mathbf{r}), \quad (17)$$

$$Q = \frac{1}{\sqrt{2}} \begin{pmatrix} c_\varphi c_\theta - is_\varphi & c_\varphi c_\theta + is_\varphi & c_\varphi c_\theta + is_\varphi & c_\varphi c_\theta - is_\varphi \\ s_\varphi c_\theta + ic_\varphi & s_\varphi c_\theta - ic_\varphi & s_\varphi c_\theta - ic_\varphi & s_\varphi c_\theta + ic_\varphi \\ \sqrt{\frac{\epsilon_0}{\mu_0}}(-s_\varphi - ic_\varphi c_\theta) & \sqrt{\frac{\epsilon_0}{\mu_0}}(s_\varphi - ic_\varphi c_\theta) & \sqrt{\frac{\epsilon_0}{\mu_0}}(-s_\varphi + ic_\varphi c_\theta) & \sqrt{\frac{\epsilon_0}{\mu_0}}(s_\varphi + ic_\varphi c_\theta) \\ \sqrt{\frac{\epsilon_0}{\mu_0}}(c_\varphi - is_\varphi c_\theta) & -\sqrt{\frac{\epsilon_0}{\mu_0}}(c_\varphi + is_\varphi c_\theta) & \sqrt{\frac{\epsilon_0}{\mu_0}}(c_\varphi + is_\varphi c_\theta) & -\sqrt{\frac{\epsilon_0}{\mu_0}}(c_\varphi - is_\varphi c_\theta) \end{pmatrix}, \quad (21)$$

where  $s_x, c_x$ , denotes  $\sin x$  and  $\cos x$  respectively,  $\theta$  is the angle of incidence of the electromagnetic waves, and  $\varphi$  is the azimuthal angle; additionally

$$A(L) = \begin{pmatrix} e^{ik_z L} & 0 & 0 & 0 \\ 0 & e^{-ik_z L} & 0 & 0 \\ 0 & 0 & e^{ik_z L} & 0 \\ 0 & 0 & 0 & e^{-ik_z L} \end{pmatrix}. \quad (22)$$

The incoming and outgoing waves on the LCE slab are related by the transfer matrix. We will denote by  $U$  the mentioned matrix associated with the elastomer slab; this matrix has the property  $\boldsymbol{\psi}(L) = U \cdot \boldsymbol{\psi}(0)$ . Below we will explain how to calculate numerically this matrix, and we will determine the explicit form of  $\boldsymbol{\psi}$  inside the LCE slab. The solution of the Maxwell equations for the whole system, that is to say, outside and inside the elastomer, can be expressed in terms of matrix  $T(z)$ , which is the transfer matrix of the complete system,

$$\begin{pmatrix} T_L \\ 0 \\ T_R \\ 0 \end{pmatrix} = T(z) \begin{pmatrix} A_L \\ R_L \\ A_R \\ R_R \end{pmatrix}, \quad (23)$$

where after substitution of the boundary conditions given in Eq. (20), we get

$$T(L) = A^{-1}(L) \cdot Q^{-1} \cdot U \cdot Q. \quad (24)$$

Finally, we will obtain the amplitudes of the reflected and transmitted waves, taking into account those corresponding to the incident waves. For each value of the polarization, for this

$$\nabla \cdot \mathbf{B}(\mathbf{r}) = 0, \quad (18)$$

$$\nabla \times \mathbf{H}(\mathbf{r}, t) = -\iota\omega\mathbf{D}(\mathbf{r}), \quad (19)$$

and we will impose boundary conditions to calculate the transfer function of the system. Continuity of the transverse components implies continuity of the vector  $\boldsymbol{\psi}(z)$ , which can be expressed as

$$\boldsymbol{\psi}(0) = Q \begin{pmatrix} A_L \\ R_L \\ A_R \\ R_R \end{pmatrix}, \quad \boldsymbol{\psi}(L) = A(L) \cdot Q \begin{pmatrix} T_L \\ 0 \\ T_R \\ 0 \end{pmatrix}, \quad (20)$$

Upon substitution of Eqs. (10), (11), (13), and (14) in the latter expressions we get the following explicit expression matrices for  $Q$  and  $A$ :

purpose, we restate Eq. (23) as

$$\begin{pmatrix} T_L \\ R_L \\ T_R \\ R_R \end{pmatrix} = S \begin{pmatrix} A_L \\ 0 \\ A_R \\ 0 \end{pmatrix}, \quad (25)$$

where  $S$  denotes the scattering matrix. For our case the elements  $S_{\ell,2}$  and  $S_{\ell,4}$  of matrix  $S$ , with  $\ell = 1, 2, 3, 4$ ; are unnecessary because we have assumed that there are no incident waves in the region  $z > L$ . Therefore the amplitudes of the transmitted and reflected waves can be expressed as

$$\begin{pmatrix} T_L \\ R_L \\ T_R \\ R_R \end{pmatrix} = \begin{pmatrix} t_{LL} & S_{12} & t_{LR} & S_{14} \\ r_{LL} & S_{22} & r_{LR} & S_{24} \\ t_{LR} & S_{23} & t_{RR} & S_{34} \\ r_{LR} & S_{24} & r_{LR} & S_{44} \end{pmatrix} \begin{pmatrix} A_L \\ 0 \\ A_R \\ 0 \end{pmatrix}, \quad (26)$$

where  $t_{nm}$  and  $r_{nm}$  ( $n, m = R, L$ ) are the transmission and reflection coefficients,  $A_{L,R}$ ,  $T_{L,R}$  and  $R_{L,R}$ , are the amplitudes of incident, transmitted, and reflected circularly polarized waves, respectively, and the subscripts  $L, R$  denote the left or right circular polarization of the waves. The copolarized transmittances are denoted by  $T_{nn} = |t_{nn}|^2$  and the cross-polarized ones by  $T_{nm} = |t_{nm}|^2$  with  $n \neq m$ , and similarly for the reflectances. These quantities are function of the incidence angle  $\theta$  and the azimuthal angle  $\varphi$ , the axial elongation  $\eta$ , and the wavelength  $\lambda$ .

## B. Maxwell equations in the region inside the LCE slab

The Maxwell equations can be stated in the Marcuvitz-Schwinger representation for the region inside the elastomer. Hence, the Maxwell equations can be written in the form

$$\frac{d}{dz} \boldsymbol{\psi}(z) = -i\mathbf{M}(z) \cdot \boldsymbol{\psi}(z), \quad (27)$$

where  $\psi(z)$  is a four-component vector, formed by the transverse components of the electromagnetic fields

$$\psi(z) = \begin{pmatrix} E_x(z) \\ E_y(z) \\ H_x(z) \\ H_y(z) \end{pmatrix}. \quad (28)$$

Here  $M(z)$  is a  $4 \times 4$  matrix, which can be written as

$$M(z) = \begin{pmatrix} 0 & 0 & -\frac{k_x k_y}{\rho \epsilon_{zz}^e} & \frac{k_x^2}{\rho \epsilon_{zz}^e} - \zeta \\ 0 & 0 & \zeta - \frac{k_y^2}{\rho \epsilon_{zz}^e} & \frac{k_x k_y}{\rho \epsilon_{zz}^e} \\ \frac{k_x k_y}{\zeta} + \rho \epsilon_{yx}^e & \rho \epsilon_{yy}^e - \frac{k_x^2}{\zeta} & 0 & 0 \\ \frac{k_y^2}{\zeta} - \rho \epsilon_{xx}^e & -\frac{k_x k_y}{\zeta} - \rho \epsilon_{xy}^e & 0 & 0 \end{pmatrix}, \quad (29)$$

where  $\rho = \epsilon_0 \omega$  and  $\zeta = \mu_0 \omega$ ,  $\epsilon_{v,\gamma}^e$  and  $v, \gamma = (x, y, z)$  correspond to elements of the dielectric tensor for the hybrid medium, and  $k_x$  and  $k_y$  are the components of the forward and backwards wave vectors.

To solve numerically Eq. (29), we shall use the piecewise constant method, which has been successfully applied to calculate optical properties of structurally chiral artificial films. In this method [33,34], an inhomogeneous material is divided into slices perpendicularly placed with respect to the inhomogeneity axis, each one of thickness  $\Delta z$ . Within each thin slice, the dielectric tensor is approximated as constant at

$$\exp \left[ iM \left( z_{j-1} + \frac{\Delta z_s}{2}, \kappa, \varphi \right) \Delta z_s \right] = I + \sum_{n=1}^{\infty} \frac{(i\Delta z_s)^n}{n!} \left[ M \left( z_{j-1} + \frac{\Delta z_s}{2}, \kappa, \varphi \right) \right]^n. \quad (34)$$

The sum of matrices of the right-hand side of this expression is calculated term by term. According to the procedure of Lakhtakia *et al.* [34] this sum is stopped when the changes in all the elements of the matrices are smaller than one part in  $10^{12}$ . It should be noted that the right-hand side of the latter expression can be calculated by diagonalizing  $M(z_{j-1} + \frac{\Delta z_s}{2}, \kappa, \varphi)$ , and it is worth mention that the eigenvalues have no other geometric multiplicity than the unity [35,36]. The precision of the piecewise constant approach is controlled by means of  $\Delta z$ . However, there is no a general formula to know in advance how thin the slices should be to achieve a particular precision degree in the calculation; therefore, we have repeated the calculation several times by increasing the number of slices each time and paying attention to the stability of the transmittances and reflectances to attain the degree of desired precision. Once  $P(L, \kappa, \varphi)$  was determined using the piecewise approximation method, the plane-wave response of the slab is obtained, so we set  $U = P(L, \kappa, \varphi)$  in Eq. (24) to finally solve Eq. (26) in order to calculate the reflectance and transmittance spectra of our system.

#### IV. RESULTS

We will apply the formalism developed in this work to calculate all the elements of the spectra of a siloxane

the center of the slice. Each slice is taken thin enough such that the difference between the dielectric tensor in contiguous slices will be quite small:

$$\psi(z, \kappa, \varphi) = e^{iM(\kappa, \varphi)\Delta z} \cdot \psi(z', \kappa, \varphi), \quad (30)$$

where  $\Delta z = z - z'$ . Thus, if  $z_{j-1}$  is the distance from the beginning of the  $j$ th slice and  $\Delta z_s$  is the thickness of the slice, the transfer of the fields can be expressed as

$$\psi(z_j, \kappa, \varphi) = \exp \left[ iM \left( z_{j-1} + \frac{\Delta z_s}{2}, \kappa, \varphi \right) \Delta z_s \right] \cdot \psi(z_{j-1}, \kappa, \varphi). \quad (31)$$

Let us denote the matrizant that describes the propagation through the  $j$ th slice by

$$P'_j(\kappa, \varphi) = \exp \left[ iM \left( z_{j-1} + \frac{\Delta z_s}{2}, \kappa, \varphi \right) \Delta z_s \right]. \quad (32)$$

Therefore, the propagation over the whole sample can be obtained from the expression

$$P(L, \kappa, \varphi) \simeq P'_{N_s}(\kappa, \varphi) \cdot P'_{N_s-1}(\kappa, \varphi) \cdot P'_{N_s-2}(\kappa, \varphi) \cdots P'_1(\kappa, \varphi), \quad (33)$$

where the number of slices  $N_s = L/\Delta z_s$  should be adequately chosen for obtaining a convergent solution.

To perform the calculation of Eq. (33) we should expand the exponential matrix shown in Eq. (32) to find

backbone chain reacting with 90 mol% and 10% of the flexible difunctional cross-linking groups (di-11UB). The rodlike mesogenic groups are present in the proportion 4:1 between the nematic 4-pentylphenyl-4'-(4-buteneoxy) benzoate and the derivative of chiral cholesterol pentanoate. Their corresponding material parameters are [9]  $r = 1.16$ ,  $L = 28.8 \mu\text{m}$ ,  $p = 428 \text{ nm}$ ,  $\epsilon_{\perp} = 1.91$ ,  $\epsilon_{\parallel} = 2.25$ ,  $\mu = 1$ , along the interval (350 nm, 700 nm) and for angles of incidence in the interval ( $0^\circ$ ,  $88^\circ$ ).

In order to analyze the influence of the dopant material, we can obtain from Eq. (8), the components of the dielectric tensor parallel and perpendicular to the helix axis of the cholesteric liquid crystal doped with randomly dispersed Ag (silver) nanospheres. The background dielectric constant, the collision angular frequency, and the relaxation rate for silver in Eq. (9) are given, respectively, by  $\epsilon_0 = 5$ ,  $\omega_p = 1.367 \times 10^{16} \text{ Hz}$ , and  $\gamma = 3.03 \times 10^{13} \text{ Hz}$  [29,37]. The imaginary parts of the components are shown in the Fig. 2; Fig. 2(a) corresponds to the perpendicular component, and the parallel is shown in Fig. 2(b); we found that a small amount of metallic inclusions modifies the dielectric response of the sample, that is to say, the filling factor of dopant is less or equal than 1%. We can observe a resonant behavior around 410 nm, manifested like narrow peaks, whose thicknesses are approximately 15 nm for both components. As we show

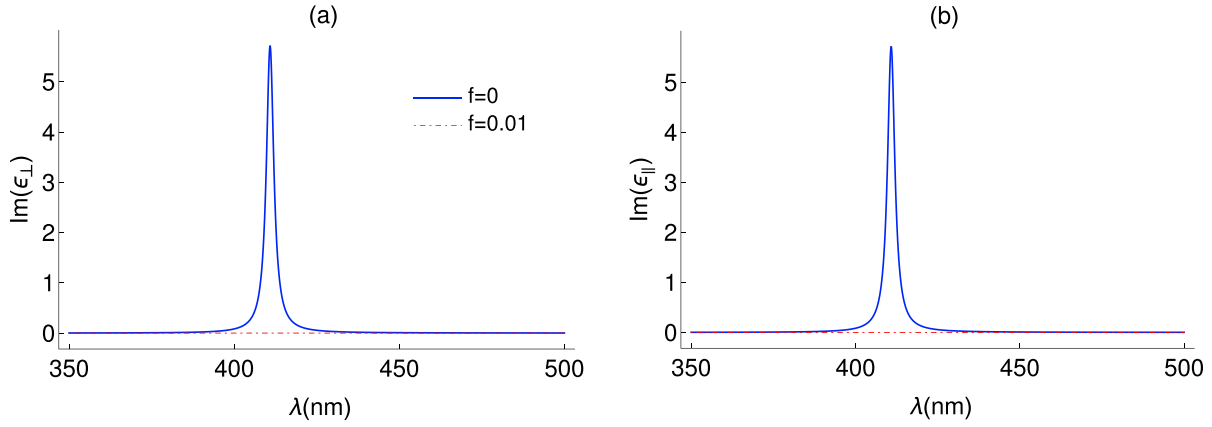


FIG. 2. Behavior of the imaginary parts of (a)  $\epsilon_{\perp}$  and (b)  $\epsilon_{\parallel}$ , for the filling factors  $f = 0$  and  $f = 0.01$ , for the interval (350 nm, 500 nm).

below, this resonance is manifested dramatically in the optical spectra of the hybrid system.

For an undistorted LCE we can clearly observe the usual circularly discriminatory behavior, which consists of allowing it to transmit the right circularly polarized field and reflect the left one; such behavior occurs in the pure system and for the filling factor  $f = 0.01$ . Also we can observe the blueshift of these structures as the incidence angle increases. When the dopant material is present, stripes of null transmittance can be observed around 400 nm for the components of the transmittance spectra,  $T_{RR}$ ,  $T_{LL}$ ,  $T_{LR}$ , because of energy absorption by the metallic spheres. The components of reflectance spectra,

$R_{RR}$ ,  $R_{LL}$ , and  $R_{LR}$ , are null in practice for all the wavelengths studied.

The transmittances and reflectances for a strain applied on an elastomer of magnitude  $\eta = 1.03$  corresponding to a pure one ( $f = 0.0$ ) and a doped one ( $f = 0.01$ ) are such that the twist angle does not depend longer linearly on the  $z$  coordinate. However, the spectra exhibit some oscillations around a linear trending. Specifically, the spectra for  $T_{RR}$  and  $R_{RR}$  exhibit, respectively, stop and reflection bands, such as in an elastomer in the undistorted state. However, these bands not only blueshift as the incidence angle increases, they also widen considerably. Additionally, some narrow bands appear

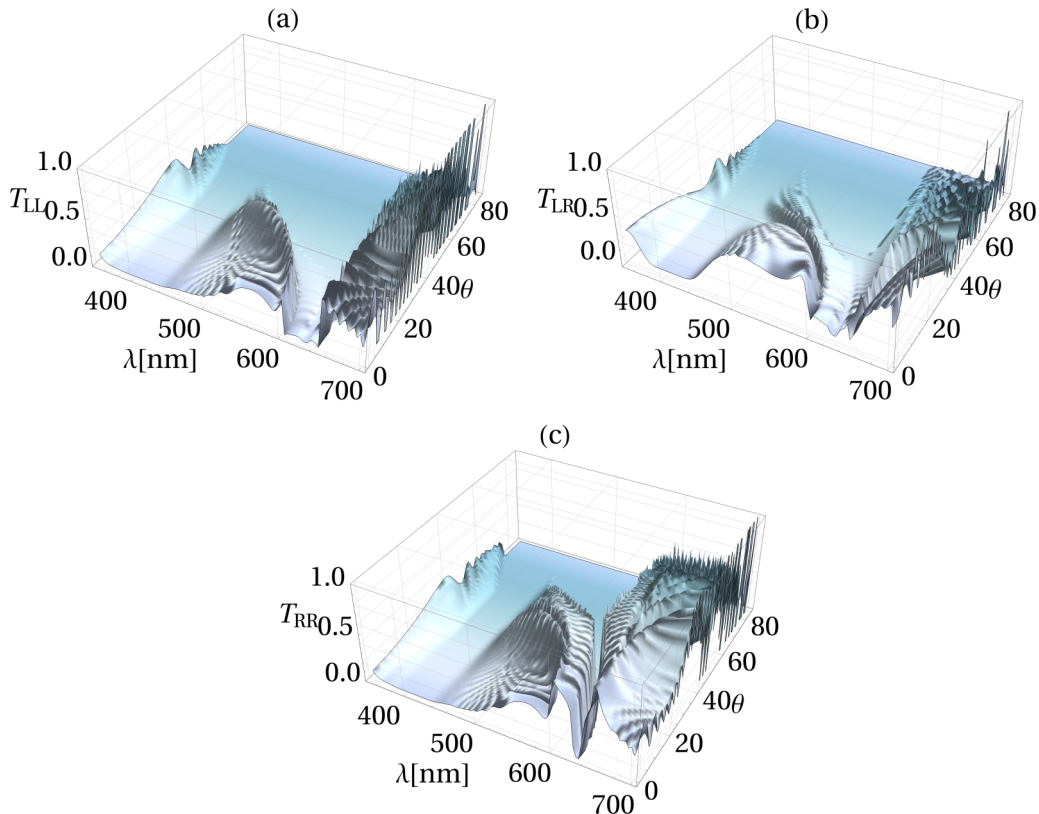


FIG. 3. Transmittance spectra (a)  $T_{LL}$ , (b)  $T_{LR}$ , and (c)  $T_{RR}$  for an elastomer stretched by  $\eta = 1.03$  doped with filling factor  $f = 0.01$ .

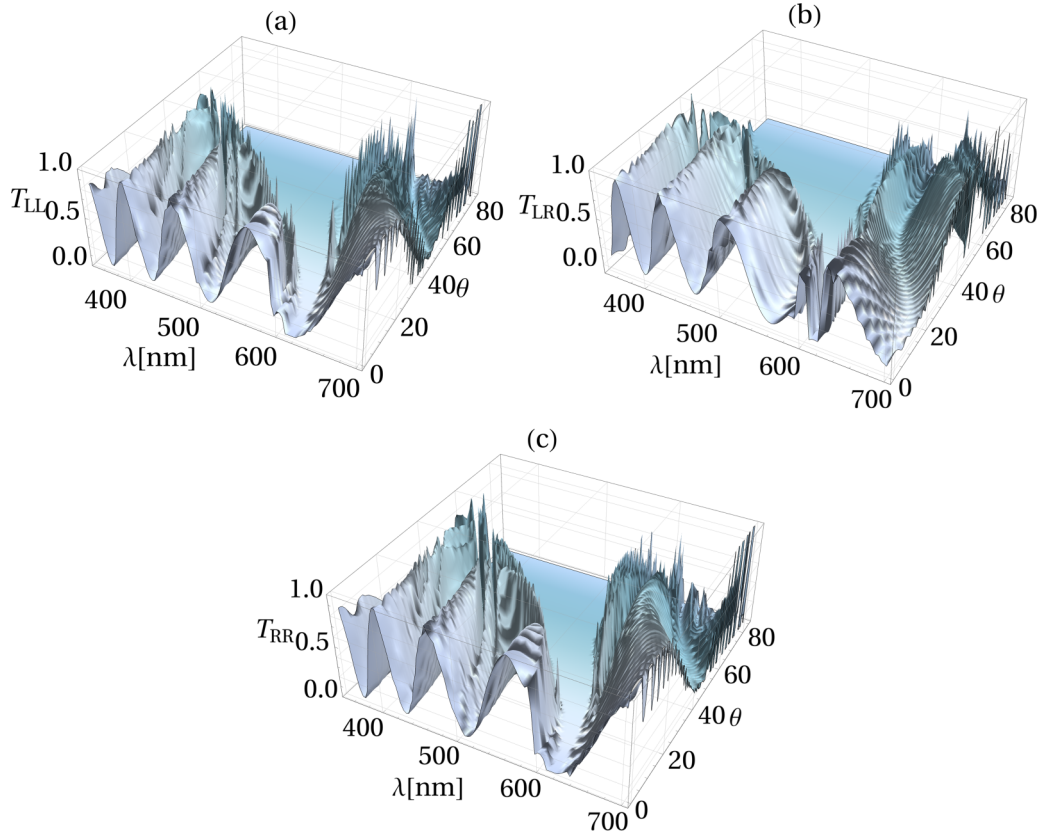


FIG. 4. The same as Fig. 2 but for  $\eta = 1.07$  and  $f = 0$ .

also for both copolarized components:  $T_{LL}$  and  $R_{LL}$ . The effect of the silver doping in  $T_{LL}$  is shown in Fig. 3(a),  $T_{LR}$  in Fig. 3(b), and  $T_{RR}$  in Fig. 3(c), which is manifested as striped shaped flat canals for both reflectances and transmittance situated around 400 nm, which are near the resonance of the metallic inclusions. These stripes, indeed, merge with the discriminatory stop bands for the larger incidence angles. These canals are present for all the spectra components and redshift lightly the reflection and stop bands just mentioned above with respect to the case without doping. In addition, we have observed that the band of conversion of a circularly left polarized wave into a right polarized one and vice versa diminishes by doping the elastomer; this band is defined by the cross-polarized transmittance  $T_{LR}$ .

We have depicted the copolarized transmittance  $T_{LL}$  in Fig. 4(a), the cross-polarized one  $T_{LR}$  in Fig. 4(b), and the copolarized one  $T_{RR}$  in Fig. 4(c); for a pure elastomer ( $f = 0.0$ ) in stretched state, the strain applied is  $\eta = 1.07$ , which is above the threshold value, therefore the helical structure is unwound. We notice that in this case,  $T_{RR}$  and  $T_{LL}$  are very similar, displaying stop bands whose bandwidths widen as the incidence angle increases. Hence, we can state the fact that the sample has a polarization-independent behavior within the reflection band located around 650 nm. On the other hand, for the component  $T_{LR}$ , we have some regions of maximum polarization conversion in the shorter wavelengths (about 400 nm), alternated with zones of polarization-independent behavior, which is also exhibited in the components  $T_{RR}$

and  $T_{LL}$  of the transmittance spectra. A comparison between Figs. 4 and 5 shows that if an LCE is doped with metallic nanospheres, omnidirectional stop bands can be observed around 400 nm for the three components of the transmittance spectra,  $T_{RR}$ ,  $T_{LL}$ , and  $T_{LR}$ , which particularly erase the conversion band that we just mentioned. All these regions are observed for an interval of incidence angles going from zero to 60°.

**V. CONCLUDING REMARKS**

We have developed a model to calculate the optical spectra of an elastomer slab doped with metallic nanospheres which is submitted to a transversely applied stress. We have obtained that once the characteristic value of stretching is overpassed, and the cholesteric arrangement has been unwound, the system switches from a discriminatory circular filter to a polarization-independent device. The system exhibits regions where the conversion from right to left circularly polarized waves is very efficient, which are alternated with regions where the transmission corresponding to both circularly polarized waves are almost indistinguishable. The specific location of each of these regions can be shifted by varying both the stretching parameter and the filling factor of the silver nanospheres.

Therefore, this tunable elastomer slab provides the possibility to build a mechanically controlled optical device which



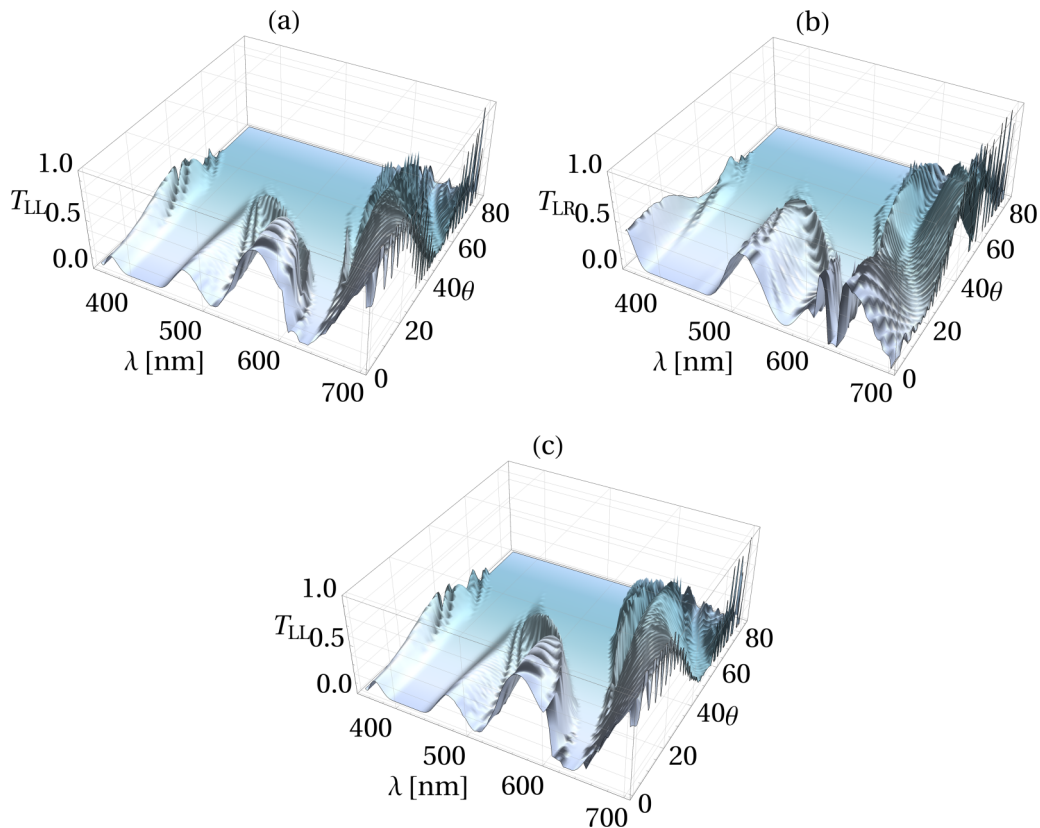


FIG. 5. The same as Fig. 2 but for  $\eta = 1.07$  and  $f = 0.01$ .

changes either from a circularly polarized selector to a mechanism that does not distinguish between polarization states or to a device which transforms from left to right circularly polarized waves. We think that our study could encourage the construction of these interesting types of devices.

#### ACKNOWLEDGMENT

This work was supported by the Mexican National Council for Science and Technology (CONACYT) through scholarship 481106, “National Scholarships” (Becas Nacionales), Program No. 000328.

- 
- [1] H. Finkelmann, H.-J. Kock, W. Gleim, and G. Rehage, *Makromol. Chem., Rapid Commun.* **5**, 287 (1984).
- [2] P. Palffy-Muhoray, in *Liquid Crystal Elastomers: Materials and Applications* (Springer, Berlin, 2012), p. 95.
- [3] H. Finkelmann, S. T. Kim, A. Muñoz, P. Palffy-Muhoray, and B. Taheri, *Adv. Mater.* **13**, 1069 (2001).
- [4] F. Castles *et al.*, *Nat. Mater.* **13**, 817 (2014).
- [5] J. Schmidtke, S. Kniesel, and H. Finkelmann, *Macromolecules* **38**, 1357 (2005).
- [6] A. Varanytsia, T. Guo, and P. Palffy-Muhoray, *Appl. Opt.* **58**, 739 (2019).
- [7] M. Warner, E. M. Terentjev, R. B. Meyer, and Y. Mao, *Phys. Rev. Lett.* **85**, 2320 (2000).
- [8] Y. Mao, E. M. Terentjev, and M. Warner, *Phys. Rev. E* **64**, 041803 (2001).
- [9] Y. Hirota, Y. Ji, F. Serra, A. R. Tajbakhsh, and E. M. Terentjev, *Opt. Express* **16**, 5320 (2008).
- [10] A. N. Oraevskii and I. E. Protsenko, *J. Exp. Theor. Phys. Lett.* **72**, 445 (2000).
- [11] J. C. W. Lee and C. Chan, *Opt. Express* **13**, 8083 (2005).
- [12] P. C. P. Hrudehy, B. Szeto, and M. J. Brett, *Appl. Phys. Lett.* **88**, 251106 (2006).
- [13] M. Thiel, M. Decker, M. Deubel, M. Wegener, S. Linden, and G. von Freymann, *Adv. Mater.* **19**, 207 (2007).
- [14] A. V. Rogacheva, V. A. Fedotov, A. S. Schwanecke, and N. I. Zheludev, *Phys. Rev. Lett.* **97**, 177401 (2006).
- [15] E. Plum, J. Zhou, J. Dong, V. A. Fedotov, T. Koschny, C. M. Soukoulis, and N. I. Zheludev, *Phys. Rev. B* **79**, 035407 (2009).
- [16] M. Decker, M. W. Klein, M. Wegener, and S. Linden, *Opt. Lett.* **32**, 856 (2007).
- [17] Y. Fan, Z. Wei, H. Li, H. Chen, and C. M. Soukoulis, *Phys. Rev. B* **88**, 241403(R) (2013).
- [18] J. K. Gansel, M. Thiel, M. S. Rill, M. Decker, K. Bade, V. Saile, G. von Freymann, S. Linden, and M. Wegener, *Science* **325**, 1513 (2009).
- [19] A. H. Gevorgyan, *Phys. Rev. E* **99**, 012702 (2019).
- [20] S. Y. Vetrov, A. Y. Avdeeva, and I. V. Timofeev, *J. Exp. Theor. Phys.* **117**, 988 (2013).
- [21] S. Y. Vetrov, M. V. Pyatnov, and I. V. Timofeev, *Phys. Solid State* **55**, 1697 (2013).

- [22] S. Y. Vetrov, M. V. Pyatnov, and I. V. Timofeev, *Phys. Rev. E* **90**, 032505 (2014).
- [23] C. G. A. no and L. O. Palomares, *Appl. Opt.* **57**, 3119 (2018).
- [24] J. C. Hernández and J. A. Reyes, *Phys. Rev. E* **96**, 062701 (2017).
- [25] G. Reyes and J. A. Reyes, *J. Phys.: Condens. Matter* **31**, 325701 (2019).
- [26] G. Reyes and J. A. Reyes, *J. Opt.* **21**, 125102 (2019).
- [27] F. Wang, A. Lakhtakia, and R. Messier, *J. Mod. Opt.* **50**, 239 (2003).
- [28] J. C. Maxwell Garnett, *Philos. Trans. R. Soc., A* **203**, 385 (1904).
- [29] S. Y. Vetrov, A. Y. Avdeeva, and I. V. Timofeev, *J. Exp. Theor. Phys.* **113**, 755 (2011).
- [30] P. G. De Gennes and J. Prost, *The Physics of Liquid Crystals* (Clarendon Press, Oxford, New York, 1993).
- [31] A. Lakhtakia, B. Michel, and W. S. Weiglhofer, *J. Phys. D: Appl. Phys.* **30**, 230 (1997).
- [32] A. Lakhtakia, *Microwave Opt. Technol. Lett.* **11**, 290 (1996).
- [33] I. Abdulhalim, R. Weil, and L. Benguigui, *Liq. Cryst.* **1**, 155 (1986).
- [34] V. C. Venugopal and A. Lakhtakia, *Proc. R. Soc. London, Ser. A* **456**, 125 (2000).
- [35] H. Hochstadt, *Differential Equations: A Modern Approach* (Dover, New York, 1975).
- [36] M. Schubert, *Phys. Rev. B* **53**, 4265 (1996).
- [37] P. B. Johnson and R. W. Christy, *Phys. Rev. B* **6**, 4370 (1972).